Hodgin, E.B., et al., 2020, A link between rift-related volcanism and end-Ediacaran extinction? Integrated chemostratigraphy, biostratigraphy, and U-Pb geochronology from Sonora, Mexico: Geology, v. 49, https://doi.org/10.1130/G47972.1

A link between rift-related volcanism and end-Ediacaran extinction? Integrated chemostratigraphy, biostratigraphy, and U-Pb geochronology from Sonora, Mexico: SUPPLEMENTAL MATERIAL

Eben B. Hodgin[1*], Lyle L. Nelson[2*], Corey J. Wall[3], Arturo J. Barrón-Díaz[4], Lucy C. Webb[2], Mark D. Schmitz[3], David A. Fike[5], James W. Hagadorn[6], Emily F. Smith[2]

[1]*Deptartment of Earth and Planetary Sciences, Harvard University, Cambridge, MA 02138 USA*

[2]*Department of Earth and Planetary Sciences, Johns Hopkins University, Baltimore, MD 21218 USA*

[3]*Department of Geosciences, Boise State University, Boise, ID 83725 USA*

[4]*Departamento de Geología, Universidad de Sonora (UNISON), Hermosillo, 83000 Mexico*

[5]*Department of Earth and Planetary Sciences, Washington University, St. Louis, MO 63130 USA*

[6]*Department of Earth Sciences, Denver Museum of Nature & Science, Denver, CO 80205 USA*

[*]ebenblake@berkeley.edu, lylelnelson@jhu.edu.

This Supplemental Material includes:

1) Section S1: Detailed methods (carbonate $\delta^{13}C$ and $\delta^{18}O$ isotopes, mineral separation and imaging, LA-ICPMS and CA-ID-TIMS U-Pb zircon geochronology);
2) Section S2: Diagenetically-altered tuffaceous deposits in marine carbonates;

3) Three supplemental tables (carbonate $\delta^{13}C$ and $\delta^{18}O$ isotopes, LA-ICPMS U-Pb data, CA-ID-TIMS U-Pb data); and
4) Five supplemental figures (carbonate C-O isotope cross-plot, lithic tuff photomicrographs, U-Pb Concordia and kernel density plots, 540 Ma zircon trace element geochemistry, and zircon CL images).

SECTION S1: DETAILED METHODS

Carbonate Stable Isotopes

Fist-sized carbonate samples were collected from measured stratigraphic sections, and fresh cut surfaces were microdrilled for powder along laminations, avoiding alteration textures. Samples from sections LV1801, LV1802, CC1801, CC1802, and CR1801 were analyzed at the Johns Hopkins University, while samples from sections CR1705, CR1804, and CR1805 were analyzed at Washington University in St. Louis.

At the Johns Hopkins University Department of Earth and Planetary Sciences Isotope Ratio Mass Spectrometer Laboratory, carbonate samples were analyzed for carbon and oxygen isotopic compositions ($\delta^{13}C$, $\delta^{18}O$) using a GasBench II peripheral device coupled to a Thermo-Finnigan MAT253 isotope ratio mass spectrometer (IRMS) in continuous-flow mode. Approximately 0.3 mg of sample carbonate powder reacted with 100% phosphoric acid in helium-purged vials at 30°C, overnight. Evolved CO_2 gas was then analyzed against tank CO_2 gas and isotopic results normalized to V-PDB (Vienna-Pee Dee Belemnite) per mil (‰) scale using working in house carbonate standards (ICM, Carrara Marble and IVA Analysentechnik, calcium carbonate) that are calibrated against international standards NBS-18 and IAEA-603. A 30°C acid fractionation factor of -1.42‰ was added to normalized dolomite $\delta^{18}O$ values (Rosenbaum and Sheppard, 1986; Kim

et al., 2007). Standard deviation (1σ) of $\delta^{13}C$ and $\delta^{18}O$ values for in house standards was <0.02‰ and <0.14‰, respectively.

At Washington University in St. Louis, carbonate samples were prepared for carbon and oxygen isotopic analyses by dissolving ~100 μg in 100% phosphoric acid (H_3PO_4) for at least 4 hours at 70°C. Sample vials were subsequently flushed with He and the evolved CO_2 was measured on a Thermo Finnigan Gasbench II coupled to a Delta V Advantage IRMS. Carbon and oxygen isotopes are expressed in standard delta notation ($\delta^{13}C$, $\delta^{18}O$) in per mil (‰) as a deviation from the V-PDB standard by calibration against NBS 19, NBS 20, and two in-house standards. A 70°C acid fractionation factor of -1.21‰ was added to normalized dolomite $\delta^{18}O$ values (Rosenbaum and Sheppard, 1986; Kim et al., 2007). From standard and replicate measurements, the 1σ error on $\delta^{13}C$ is <0.15‰ and $\delta^{18}O$ is <0.2‰.

Mineral Separation and Zircon Imaging

Zircon grains were separated from rock samples using a sledge, Retsch DM200 disc mill, 500 μm sieve, and Wilfley Shaker Table at Harvard University. Separation proceeded using a Frantz magnetic separator and methylene iodide heavy liquid at Massachusetts Institute of Technology. Heavy mineral separates were annealed at 900°C for >48 hours in a muffle furnace. Grains were mounted in epoxy and polished. At the University of California Santa Barbara (USCB), a Centaurus cathodoluminescence (CL) detector attached to an FEI Quanta 400f field-emission scanning electron microscope (SEM) was used to obtain CL images of polished and carbon-coated grain mounts. At Boise State University (BSU), CL images of zircon were obtained with a JEOL JSM-300 SEM in combination with a Gatan MiniCL.

LA-ICPMS U-Pb Zircon Geochronology

At UCSB, zircon U-Pb geochronology and trace element analysis was carried out by laser ablation inductively coupled plasma mass spectrometry (LA-ICPMS) using a Photon Machines Excite 193 nm Excimer laser coupled with a Nu Plasma 3D MC-ICPMS and Agilent 7700X quadrupole ICPMS, following the methods of Kylander-Clark et al. (2013). For each analysis, a 25 μm spot size was ablated at 4 Hz for 15 seconds with a 20 second washout, following 2 shots of pre-ablation, using a fluence of ~1 J/cm^2. The primary standards were 91500 (1062.4 ± 0.4 Ma) (Wiedenbeck et al., 1995) and GJ-1 (Jackson et al., 2004) for calibration of age and trace element composition, respectively. Bias and drift in U-Pb ratios were corrected using the program Iolite (Paton et al., 2010) following procedures detailed in Kylander-Clark et al. (2013). Plešovice was used as a secondary age standard (337.13 ± 0.37 Ma) (Sláma et al., 2008), and yielded a ^{206}Pb/^{238}U weighted mean date of 334.8 ± 1.0 Ma (MSWD = 1.8, n = 10). This internal uncertainty was not propagated for systematic biases.

At BSU, zircon was analyzed by LA-ICPMS using a ThermoElectron X-Series II quadrupole ICPMS and New Wave Research UP-213 Nd:YAG UV laser ablation system. Analytical protocols, standard materials, and data reduction software developed at BSU were used for acquisition and calibration of U-Pb dates and a suite of high field strength elements (HFSE) and rare earth elements (REE). Zircon were ablated with a laser spot 16 μm wide using fluence and pulse rates of 5 J/cm^2 and 10 Hz, respectively, during a 45 second analysis (15 second gas blank, 30 second ablation) excavating a pit 25 μm deep. Ablated material was carried to the nebulizer flow of the plasma by a 1.2 L/min He gas stream. Total sweep duration is 950 ms, and quadrupole dwell times were 5 ms for Si and Zr, 40 ms for ^{202}Hg, ^{204}Pb, ^{208}Pb, ^{232}Th, and ^{238}U, 80 ms for ^{206}Pb, 200 ms for ^{49}Ti and ^{207}Pb, and 10 ms for all other HFSE and REE. Background count

rates were obtained prior to each spot analysis and subtracted from the raw count rate for each analyte. For concentration calculations, background-subtracted count rates were internally normalized to ^{29}Si and calibrated with the primary standards NIST SRM-610 and -612 glasses. Ablation pits that intersected mineral inclusions were identified based on Ti and P excursions, and associated sweeps were discarded. U-Pb dates from these analyses were retained if U-Pb ratios appeared to have been unaffected by the inclusions. Mass 204 signals were typically indistinguishable from zero following subtraction of Hg backgrounds, and dates are thus reported without common Pb correction. The Ti-in-zircon thermometer was calculated using an average TiO_2 activity value of 0.8 in crustal rocks (Watson et al., 2006).

Zircon U-Pb data were collected in laser ablation experiments on January 6th, 2019 at UCSB and on August 19th, 2019 at BSU. For U-Pb and $^{207}Pb/^{206}Pb$ dates, instrumental fractionation of the background-subtracted ratios was corrected, and dates were calibrated with respect to interspersed measurements of standards and reference materials. The primary standard Plešovice zircon (Sláma et al., 2008) was used to monitor time-dependent instrumental fractionation based on two analyses for every 10 analyses of unknown zircon. Secondary standards were also analysed twice for every 10 unknowns, and a secondary correction was applied to the $^{206}Pb/^{238}U$ dates using Seiland (530 Ma) and Zirconia (327 Ma).

Radiogenic isotope ratio and age error propagation for all analyses includes uncertainty contributions from counting statistics and background subtraction. These uncertainties are the local standard deviations of the polynomial fits to the interspersed primary standard measurements versus time for the time-dependent, relatively larger U-Pb fractionation factor, and the standard errors of the means of the consistently time-invariant and smaller $^{207}Pb/^{206}Pb$ fractionation factor. These uncertainties are 1-5% (average of 2%) (2σ) for $^{206}Pb/^{238}U$ and 0.5-1.5% (average of 1%)

(2σ) for $^{207}Pb/^{206}Pb$. Errors on dates from individual analyses are given at 2σ, and zircon LA-ICPMS results are in Table S2.

CA-ID-TIMS U-Pb Zircon Geochronology

U-Pb dates were obtained by the chemical abrasion isotope dilution thermal ionization mass spectrometry (CA-ID-TIMS) method from analyses composed of single zircon grains or fragments of grains, modified after (Mattinson, 2005). Annealed zircon was removed from the epoxy mounts based on LA-ICPMS data and CL image screening. Single grains or fragments were transferred to 3 ml Teflon PFA beakers, loaded into 300 µl Teflon PFA microcapsules with 120 µl of 29 M HF, placed in a large-capacity Parr vessel, and partially dissolved for 12 hours at 190°C.

The zircon grains or fragments were returned to 3 ml Teflon PFA beakers, HF removed, and rinsed in ultrapure H_2O, immersed in 3.5 M HNO_3, ultrasonically cleaned for one hour, and fluxed at 80°C for one hour. The HNO_3 was removed and grains or fragments were rinsed twice in ultrapure H_2O, then reloaded into Teflon PFA and spiked with Boise State BSU1B tracer solution with a calibration of $^{235}U/^{205}Pb = 77.93$ and $^{233}U/^{235}U = 1.007066$. Zircon was dissolved in Parr vessels in 120 µl of 29 M HF at 220°C for 48 hours, dried to fluorides, and re-dissolved in 6 M HCl at 180°C overnight. Uranium and Pb were separated from the zircon matrix using an HCl-based anion-exchange chromatographic procedure (Krogh, 1973), eluted together, and dried with 2 µl of 0.05 N H_3PO_4.

Uranium and Pb were loaded on a single outgassed Re filament in 5 µl of a silica-gel/phosphoric acid mixture (Gerstenberger and Haase, 1997), and U and Pb isotopic measurements made on a GV IsotopX Phoenix multicollector thermal ionization mass spectrometer equipped with an ion-counting Daly detector. Pb isotopes for analyses with smaller

amounts of radiogenic Pb were measured by peak-jumping all isotopes on the Daly detector for 150 cycles, and corrected for 0.16 ± 0.06/a.m.u. (2σ) mass fractionation. Pb isotopes for analyses with larger amounts of radiogenic Pb were measured by a Faraday-Daly routine that cycles 150-200 times between placing mass 204 in the axial Daly collector and masses 205-208 on the H1-H4 Faraday detectors to placing mass 205 in the axial Daly and masses 206-208 in the H1-H3 Faradays, providing real-time Daly gain correction. These results were corrected for 0.10 ± 0.06%/a.m.u. (2σ) mass fractionation. Transitory isobaric interferences due to high-molecular weight organics, particularly on ^{204}Pb and ^{207}Pb, disappeared within approximately 30 cycles. The ionization efficiency of each Pb isotope averaged 10^4 cps/pg. Linearity (to ≥1.4 x 10^6 cps) and the associated deadtime correction of the Daly detector were monitored by repeated analyses of NBS982. Uranium was analyzed as UO_2^+ ions in static Faraday mode on 10^{11} or 10^{12} ohm resistors for 200-300 cycles, and corrected for isobaric interference of $^{233}U^{18}O^{16}O$ on $^{235}U^{16}O^{16}O$ with an $^{18}O/^{16}O$ of 0.00206. Ionization efficiency averaged 20 mV/ng of each U isotope. Uranium mass fractionation was corrected using the known $^{233}U/^{235}U$ ratio of the tracer solutions.

CA-ID-TIMS U-Pb dates and uncertainties were calculated using the algorithms of (Schmitz and Schoene, 2007), and U decay constants recommended by (Jaffey et al., 1971). $^{206}Pb/^{238}U$ ratios and dates were corrected for initial ^{230}Th disequilibrium using a Th/U[magma] = 3.0 ± 0.3, resulting in an increase in the $^{206}Pb/^{238}U$ dates of ~0.09 Ma. All common Pb in analyses was attributed to laboratory blank and subtracted based on the measured laboratory Pb isotopic composition and associated uncertainty. Uranium blanks were estimated at 0.013 pg.

CA-ID-TIMS weighted mean $^{206}Pb/^{238}U$ dates were calculated from equivalent dates (pof >0.05) using Isoplot 3.0 (Ludwig, 2003). Errors on the weighted mean dates are given as ± x / y / z, where x is the internal error based on analytical uncertainties only, including counting statistics,

subtraction of tracer solution, and blank and initial common Pb subtraction, y includes the tracer calibration uncertainty propagated in quadrature, and z includes the ^{238}U decay constant uncertainty propagated in quadrature. Internal errors should be considered when comparing our dates with $^{206}Pb/^{238}U$ dates from other laboratories that used the same EARTHTIME tracer solution or a tracer solution that was cross-calibrated using EARTHTIME gravimetric standards. Errors including the uncertainty in the tracer calibration should be considered when comparing our dates with those derived from other geochronological methods using the U-Pb decay scheme (for example LA-ICPMS). Errors including uncertainties in the tracer calibration and ^{238}U decay constant (Jaffey et al., 1971) should be considered when comparing our dates with those derived from other decay schemes (for example $^{40}Ar/^{39}Ar$, ^{187}Re-^{187}Os). Errors for weighted mean dates and dates from individual grains are given at 2σ and shown in Table S3.

SECTION S2: DIAGENETICALLY-ALTERED TUFFACEOUS DEPOSITS IN MARINE CARBONATES

There are millimetric domains preserved within two thin sections of the dated sandy dolostone sample, CC1801-138, that are composed of a combination of finer grained (than the matrix) light green clay minerals, dolomite rhombs, hematite, secondary quartz, and porosity (Fig. S2D-G). These domains are interpreted as intraclasts that contain the same peloidal dolomite textures as the matrix. Therefore, the porosity associated with these intraclasts (evidenced by sparry dolomite and silica crystallization) may be due to dolomite replacement of primary calcite. Alternatively, these features are also consistent with an originally tuffaceous vitroclastic matrix of replaced and devitrified glass and secondary mineral infilling of original porosity. Similar diagenetic features and textures associated with originally tuffaceous components have

previously been observed in marine carbonate rocks. For example, biotite rich layers in pelagic carbonate successions from the Eocene-Oligocene of the Mediterranean basin have been identified as mineral relicts of ashfall deposits (Odin et al., 1991; Coccioni et al., 2008; Sahy et al., 2017). Altered clay-size fractions of illite, chlorite, and biotite associated with tuffs have also been documented from beds having undergone burial diagenesis (Ullah et al., 2020). Hematite pigment and neomorphism has also been reported, in association with altered clay in Paleozoic to Mesozoic marine tuffs (Kiipli et al., 2000; Chakraborty et al., 2018). In sample CC1801-138, petrographic evidence for alteration of clay and clay minerals to hematite, and evidence for clay-rich intraclasts with original porosity and abundant secondary silica, may thus be related to a minor component of reworked and diagenetically altered silicate ash. Such an interpretation is consistent with the characteristics and quality of the zircon crystals from the dated rock sample that make up a near-depositional population of reproducible $^{206}Pb/^{238}U$ dates at 539.40 ± 0.23 Ma.

SUPPLEMENTAL MATERIAL TABLE CAPTIONS

Table S1. Carbonate $\delta^{13}C$ and $\delta^{18}O$ isotopic data.

Table S2. LA-ICPMS U-Pb geochronologic analyses and trace element concentrations.

Table S3. CA-ID-TIMS U-Th-Pb isotopic data.

SUPPLEMENTAL MATERIAL FIGURES

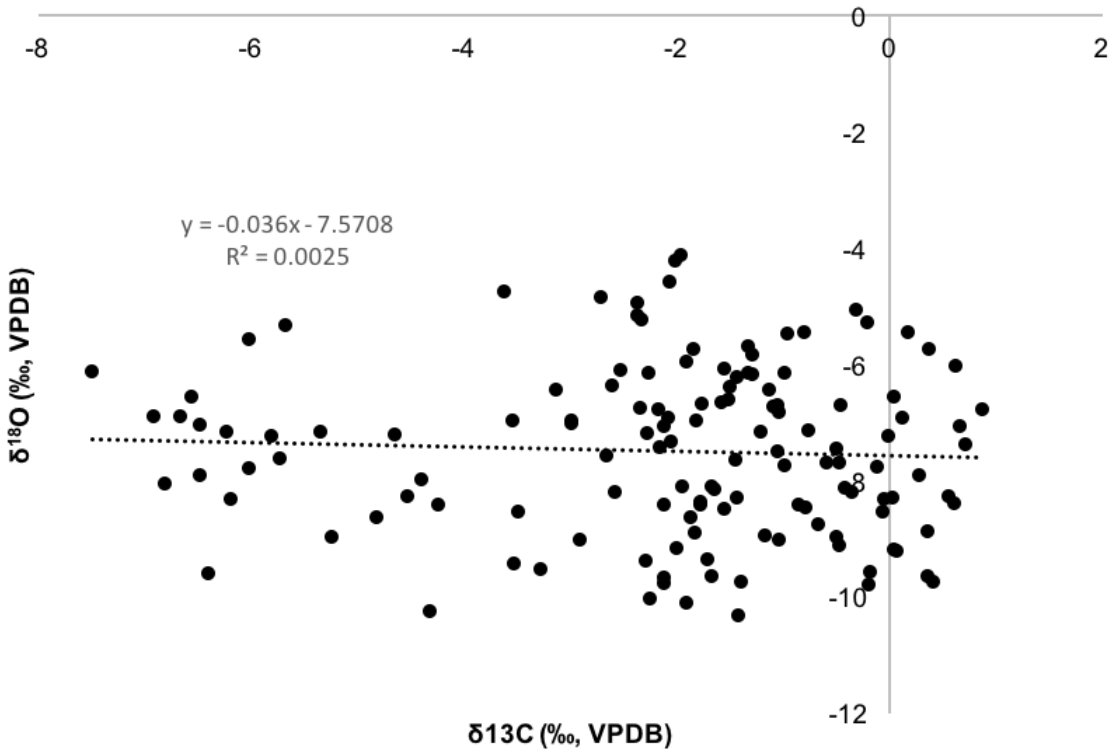

Figure S1. Carbon-oxygen isotope cross plot from the La Ciénega Fm. The dotted black line is a linear regression fitted to the data (Fig. 1 and Table S1) with an R^2 value of 0.0025.

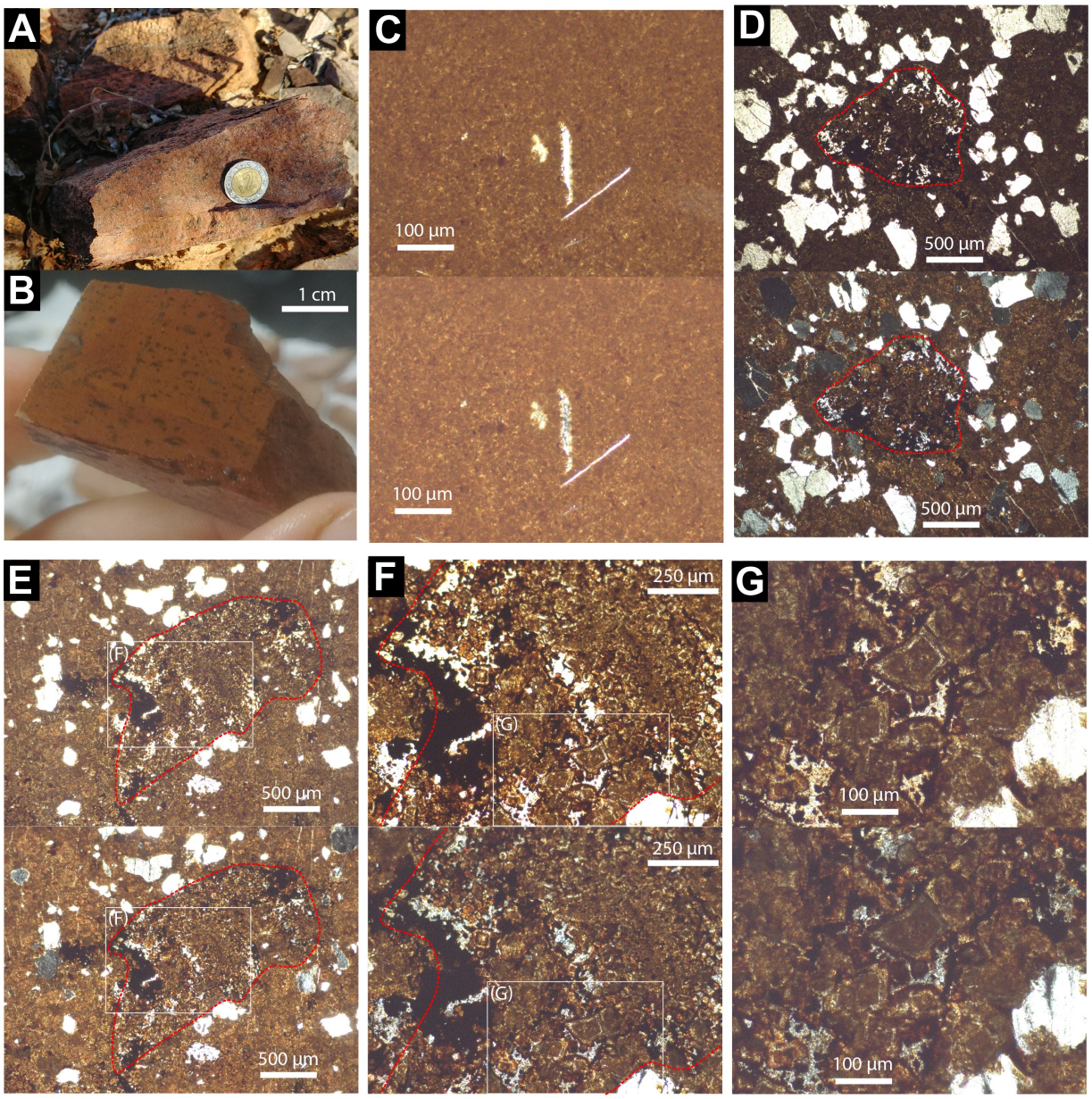
A
B
1 cm
C
100 µm
100 µm
D
500 µm
500 µm
E
(F)
500 µm
(F)
500 µm
F
250 µm
(G)
250 µm
(G)
G
100 µm
100 µm

207

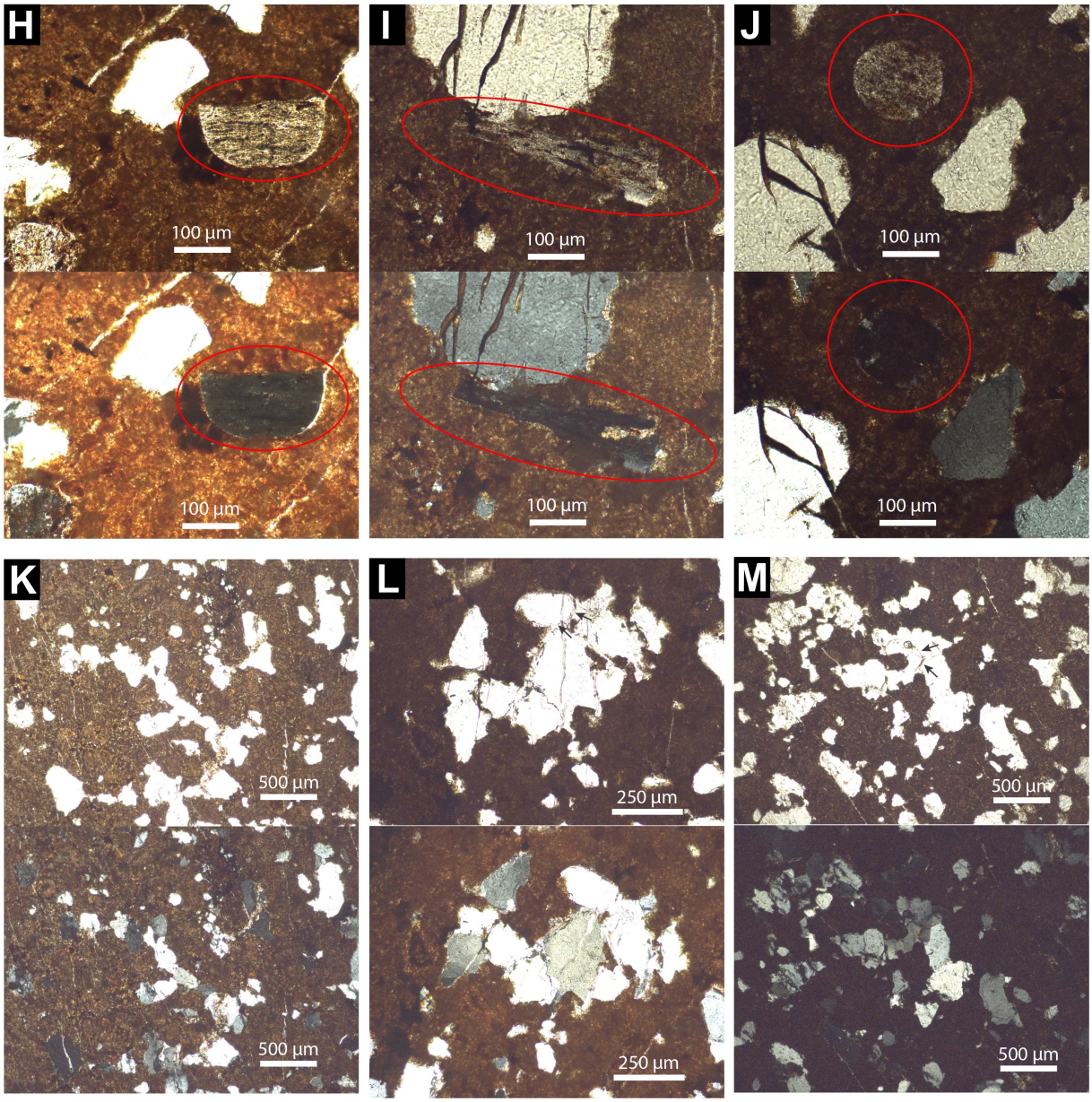

Figure S2. Photographs and Photomicrographs of U-Pb sample CC1801-138. Sets of photomicrographs (C-M) are displayed in plane-polarized light (above) and cross-polarized light (below). (A) Field photograph of 10-cm thick sandy dolostone bed from which CC1801-138 was sampled. Coin for scale, 12.85 mm diameter. (B) Hand sample displaying fine-grained dolomitic matrix with well-developed internal lamination. (C) Fine-grained peloidal dolomicrite. (D-G) Coarse-grained millimetric intraclasts of peloidal and sparry dolostone with secondary mineral infilling of original porosity and hematization of clay minerals, similar to features observed in devitrified and diagenetically altered tuffaceous horizons in marine carbonates (Section S2). Red dashed line indicates boundary of intraclasts. (H-J) Rounded accidental lithics of basement-derived metamorphic rock fragments, identified within red circles. (K-M) Irregularly-shaped (amoeboid) clusters of rounded to sub-rounded quartz grains displaying quartz overgrowths with

internal dust lines, provide evidence for derivation from older, quartz-rich sedimentary rocks. Dust lines are indicated by black arrows.

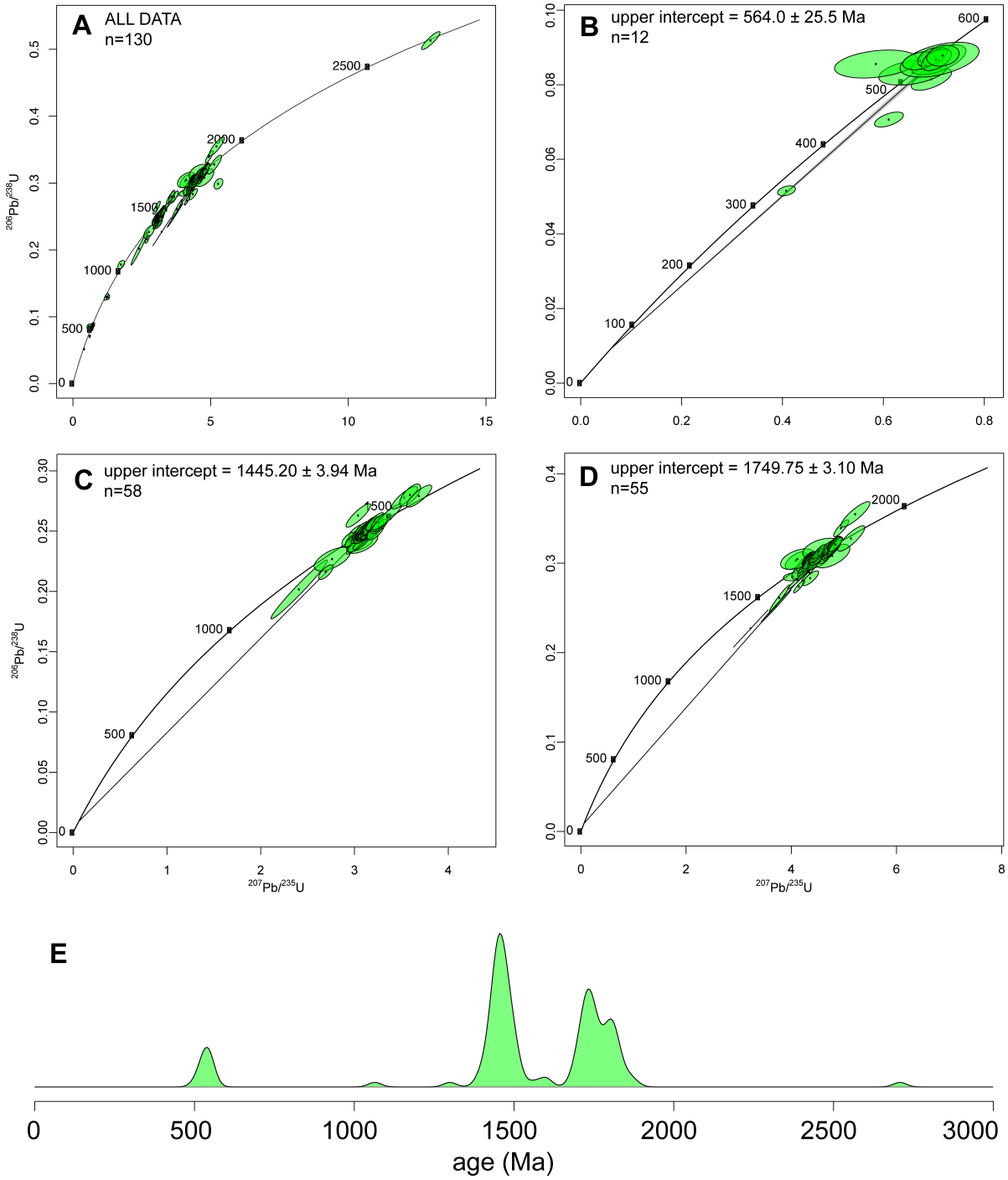

Figure S3. CC1801-138 LA-ICPMS U-Pb Concordia and Kernel Density Estimation plots. (A) U-Pb Concordia plot of all data. (B-D) U-Pb Concordia plots of *circa* 540, 1450, and 1750 Ma age populations, respectively. Discordia lines are anchored at 60 Ma, when peak metamorphism

occurred (González-León et al., 2017; Barrón-Díaz et al., 2019). (E) Kernel Density Estimation (KDE) plot of all concordant data (119 of 130 analyses). KDE includes a 900 Ma cutoff for $^{206}Pb/^{238}U$ to $^{207}Pb/^{206}Pb$ age calculations. $^{206}Pb/^{238}U$ dates were excluded when discordance ($^{206}Pb/^{238}U$ vs. $^{207}Pb/^{235}U$) was >25%. $^{207}Pb/^{206}Pb$ dates were excluded when discordance ($^{206}Pb/^{238}U$ vs. $^{207}Pb/^{206}Pb$) was <-10% or >+15%. Plots generated using *IsoplotR* (Vermeesch, 2018).

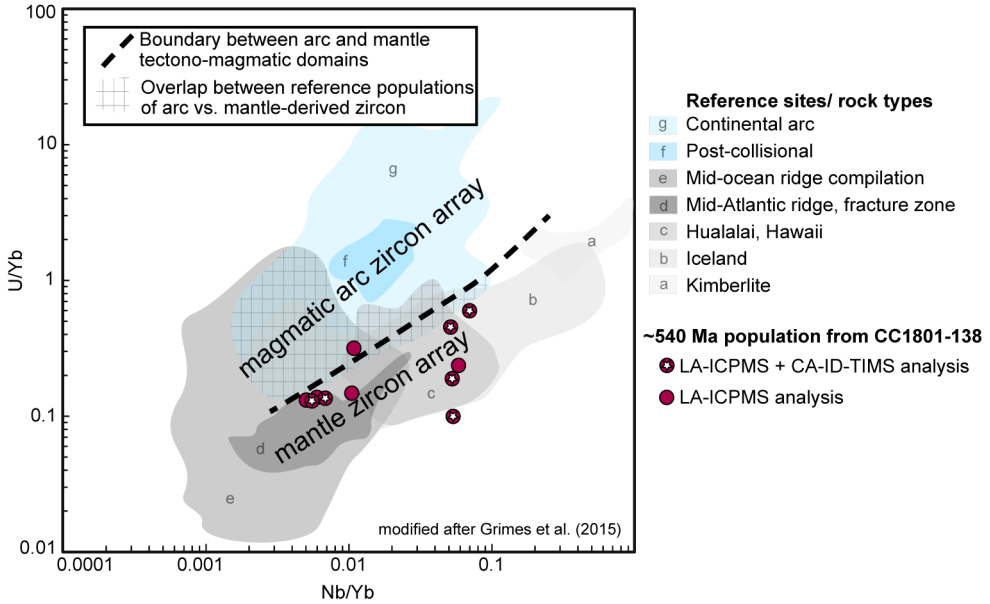

Figure S4. *Circa* 540 Ma mantle-derived zircon trace element geochemistry. Nb/Yb vs. U/Yb trace element data from the *circa* 540 Ma population of zircon within the dated sample CC1801-138, plotted against reference data of known tectono-magmatic setting (Grimes et al., 2015).

240

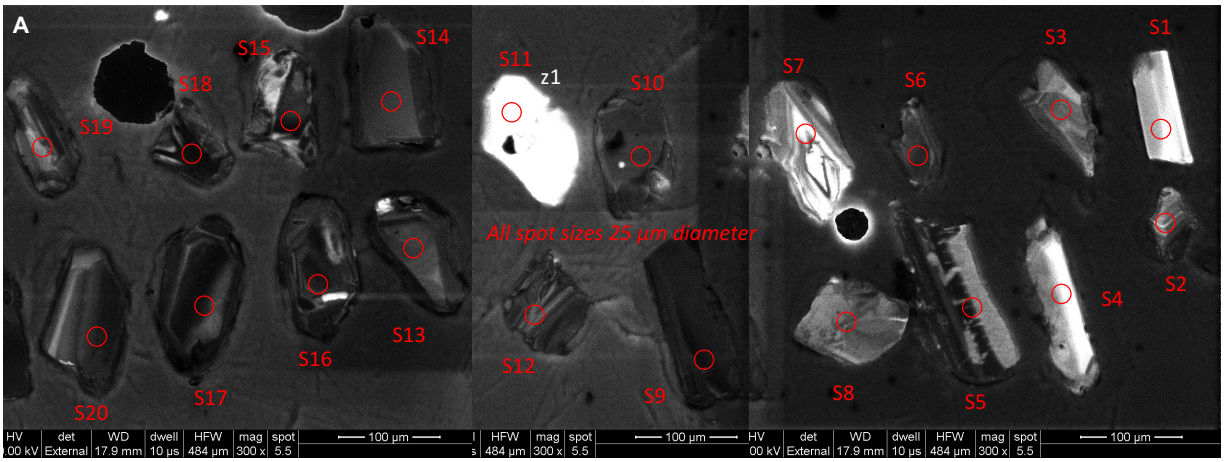

241

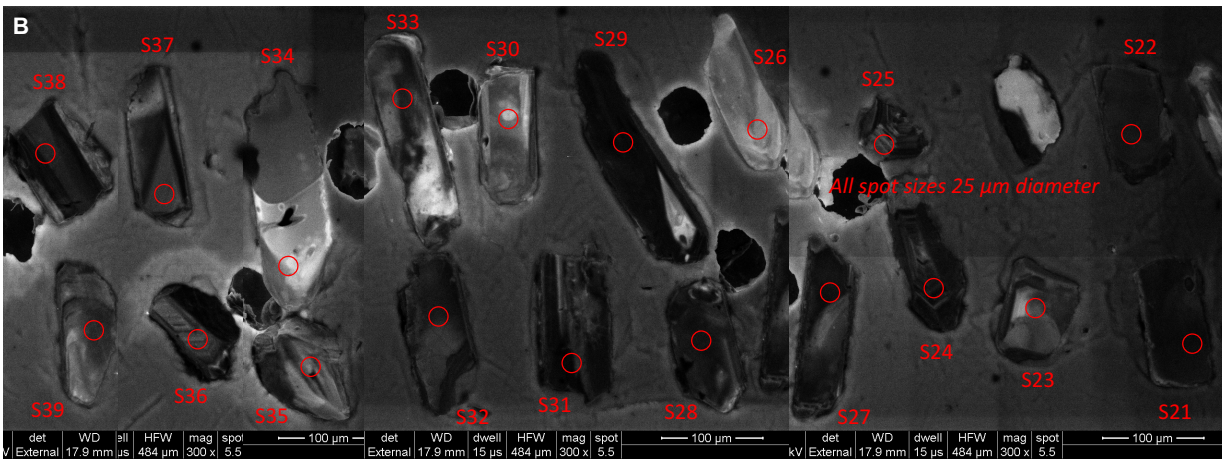

242

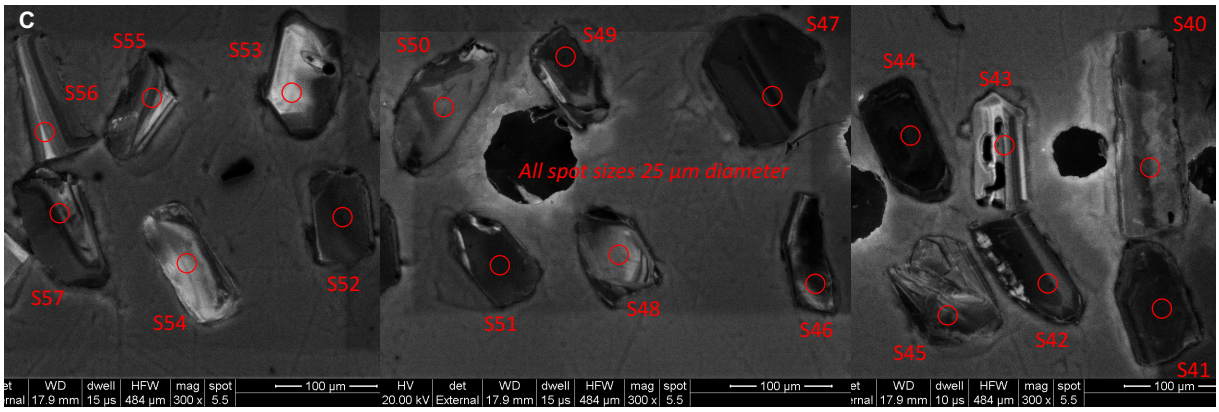

243

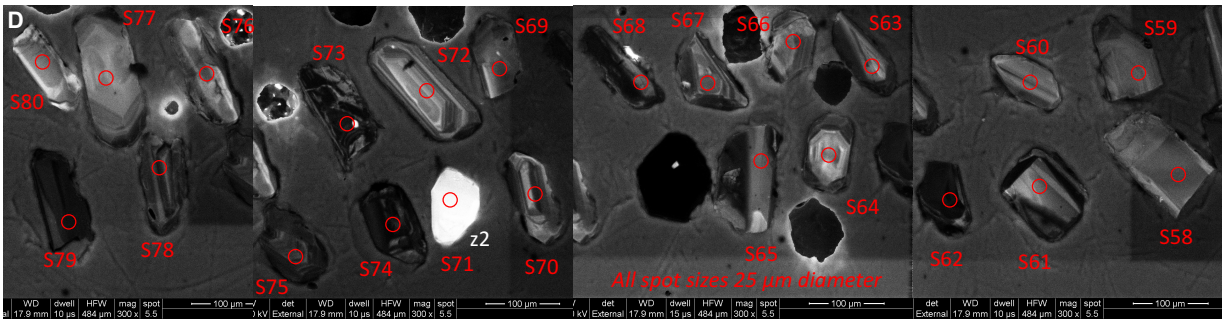

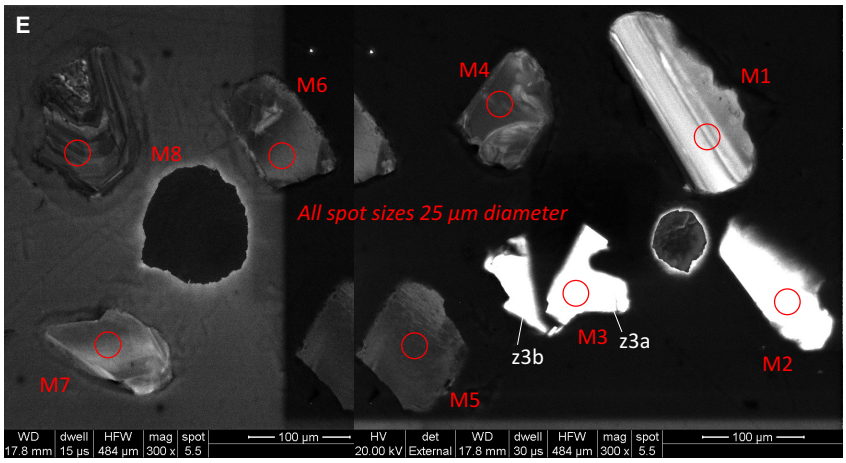

244

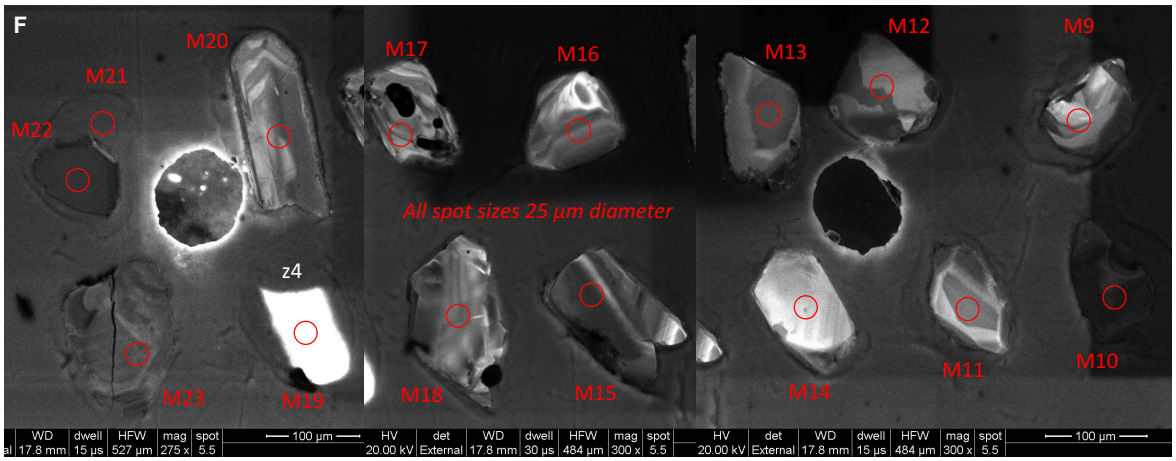

245

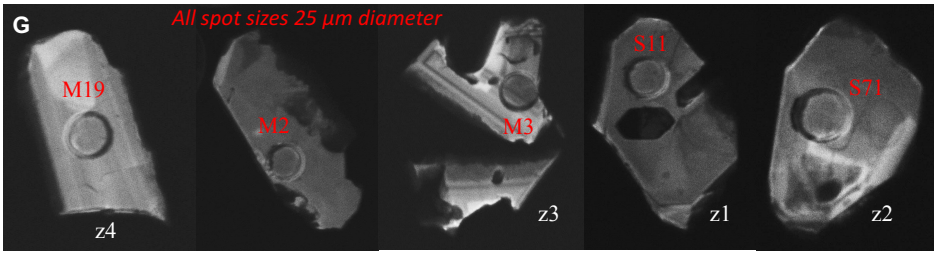

246

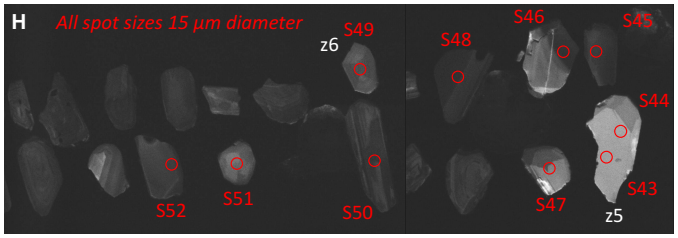

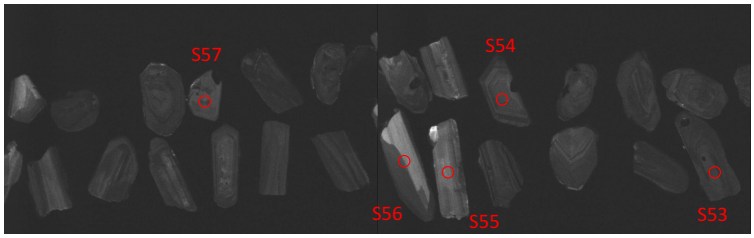

247

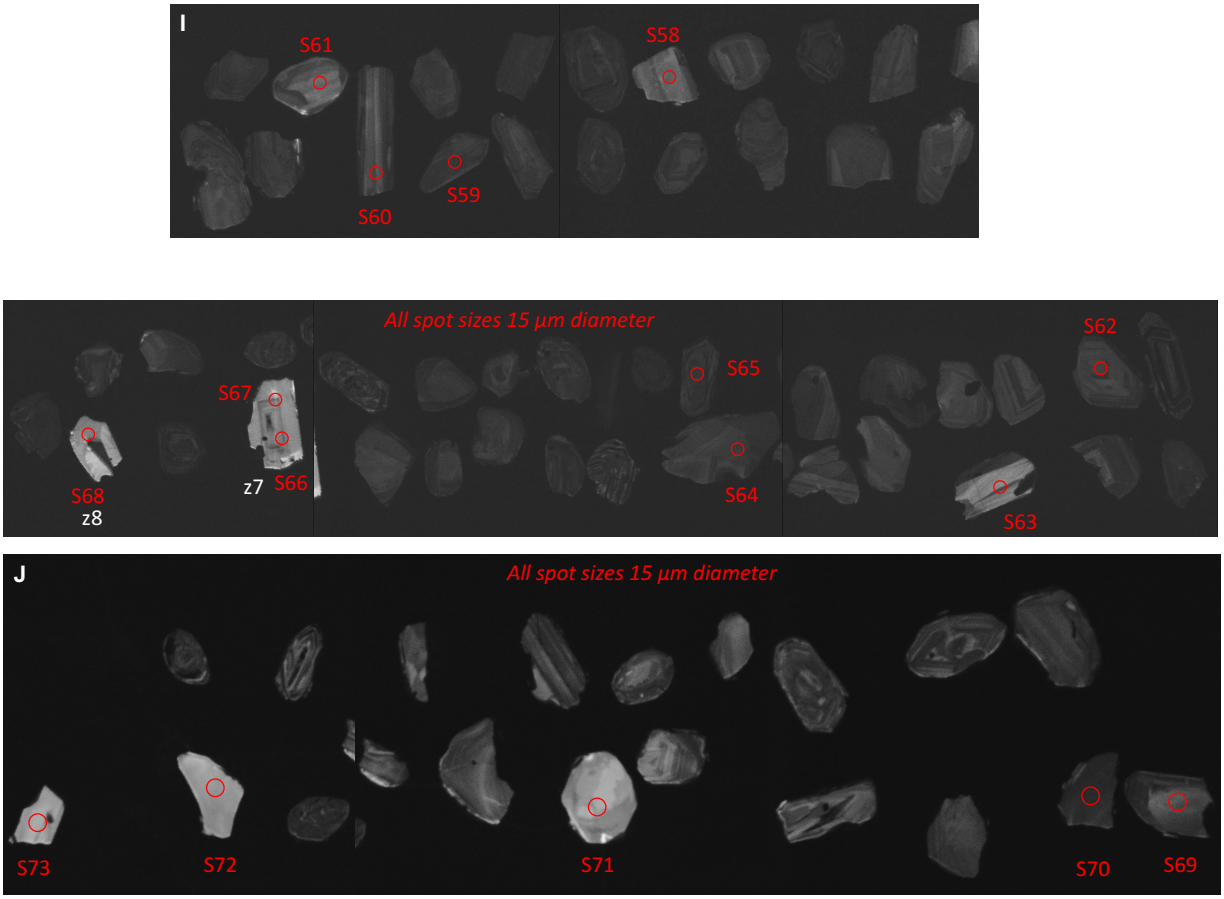

Figure S5. Zircon Cathodoluminescence (CL) images from dated sample CC1801-138. (A-D) Analyses S1-S80. Spot sizes 25 µm. Imaged at UCSB (Jan 2019) from small mount EBH2019. (E-F) Analyses M1-M23. Spot sizes 25 µm. Imaged at UCSB (Jan 2019) from medium mount EBH2019. (G) Select zircon grains re-imaged at BSU (Jan 2019) from EBH2019 mounts. (H-I) Analyses S43-S68. Spot sizes 15 µm. Imaged at BSU (Aug 2019) from small mount Blake2019B. (J) Analyses XS69-XS73. Spot sizes are 15 µm. Imaged at BSU (Aug 2019) from extra small mount Blake2019B. All labeled laser ablation spots correspond to LA-ICPMS analyses in Table S2. Zircons selected for CA-ID-TIMS indicated by z1-z5, and z7.

REFERENCES CITED

Barrón-Díaz, A.J., Paz Moreno, F.A., Miggins, D.P., and Iriondo, A., 2019, Geochronology and geothermometry of the Laramide metamorphism in the Cambrian metabasalts from the Cerro Rajón Formation, Caborca region, northwest Mexico: Journal of South American Earth Sciences, v. 91, p. 47–56, doi:10.1016/j.jsames.2019.01.005.

Chakrabarty, S., Verma, S.K., and Shukla, M., 2018, Facies Analysis, Depositional Regime & Sedimentation Processes in Mahanadi Basin: ONGC Bulletin, v. 53, p. 35–61.

Coccioni, R., Marsili, A., Montanari, A., Bellanca, A., Neri, R., Bice, D.M., Brinkhuis, H., Church, N., Macalady, A., Mcdaniel, A., Deino, A., Lirer, F., Sprovieri, M., Maiorano, P., Monechi, S., Nini, C., Nocchi, M., Pross, J., Rochette, P., Sagnotti, L., Tateo, F., Touchard, Y., Van Simaeys, S., and Williams, G.L. 2008, Integrated stratigraphy of the Oligocene pelagic sequence in the Umbria-Marche basin (northeastern Apennines, Italy): A potential Global Stratotype Section and Point (GSSP) for the Rupelian/Chattian boundary: Geological Society of America Bulletin, v. **120**, p. 487–511.

Gerstenberger, H., and Haase, G., 1997, A highly effective emitter substance for mass spectrometric Pb isotope ratio determinations: Chemical Geology, v. 136, p. 309–312, doi:10.1016/S0009-2541(96)00033-2.

González-León, C.M., Solari, L., Valencia-Moreno, M., Heimpel, M.A.R., Solé, J., Becuar, E.G., Santacruz, R.L., and Arvizu, O.P., 2017, Late Cretaceous to early Eocene magmatic evolution of the Laramide arc in the Nacozari quadrangle, northeastern Sonora, Mexico and its regional implications: Ore Geology Reviews, v. 81, p. 1137–1157, doi:10.1016/j.oregeorev.2016.07.020.

Grimes, C.B., Wooden, J.L., Cheadle, M.J., and John, B.E., 2015, “Fingerprinting” tectono-magmatic provenance using trace elements in igneous zircon: Contributions to Mineralogy and Petrology, v. 170, p. 1–26, doi:10.1007/s00410-015-1199-3.

Jackson, S.E., Pearson, N.J., Griffin, W.L., and Belousova, E.A., 2004, The application of laser ablation-inductively coupled plasma-mass spectrometry to in situ U-Pb zircon geochronology: Chemical Geology, v. 211, p. 47–69, doi:10.1016/j.chemgeo.2004.06.017.

Jaffey, A.H., Flynn, K.F., Glendenin, L.E., Bentley, W.C., and Essling, A.M., 1971, Precision measurement of half-lives and specific activities of U235 and U238: Physical Review C, v. 4, p. 1889–1906, doi:10.1103/PhysRevC.4.1889.

Kiipli, E., Kallaste, T., and Kiipli, T., 2000, Hematite and goethite in Telychian marine red beds of the East Baltic: GFF, v. 122, p. 281–286.

Kim, S.T., Mucci, A., and Taylor, B.E., 2007, Phosphoric acid fractionation factors for calcite and aragonite between 25 and 75 °C: Revisited: Chemical Geology, v. 246, p. 135–146, doi:10.1016/j.chemgeo.2007.08.005.

Krogh, T.E., 1973, A low-contamination method for hydrothermal decomposition of zircon and extraction of U and Pb for isotopic age determinations: Geochimica et Cosmochimica Acta, v. 37, p. 485–494, doi:10.1016/0016-7037(73)90213-5.

Kylander-Clark, A.R.C., Hacker, B.R., and Cottle, J.M., 2013, Laser-ablation split-stream ICP petrochronology: Chemical Geology, v. 345, p. 99–112, doi:10.1016/j.chemgeo.2013.02.019.

Ludwig, K.R., 2003, User's manual for IsoPlot 3.0. A Geochronological Toolkit for Microsoft Excel: Berkeley Geochronology Center Special Publication, v. 4, p. 70.

Mattinson, J.M., 2005, Zircon U-Pb chemical abrasion ("CA-TIMS") method: Combined annealing and multi-step partial dissolution analysis for improved precision and accuracy of zircon ages: Chemical Geology, v. 220, p. 47–66, doi:10.1016/j.chemgeo.2005.03.011.

Odin, G., Montanari, A., Deino, A., Drake, R., Guise, P., Kreuzer, H., and Rex, D, 1991, Reliability of volcano-sedimentary biotite ages across the Eocene-Oligocene boundary (Apennines, Italy): Chemical Geology, v. 86, p. 203–224.

Paton, C., Woodhead, J.D., Hellstrom, J.C., Hergt, J.M., Greig, A., and Maas, R., 2010, Improved laser ablation U-Pb zircon geochronology through robust downhole fractionation correction: Geochemistry, Geophysics, Geosystems, v. 11, no. 3, p. 1–36, doi:10.1029/2009GC002618.

Rosenbaum, J., and Sheppard, S.M.F., 1986, An isotopic study of siderites, dolomites and ankerites at high temperatures: Geochimica et Cosmochimica Acta, v. 50, no. 6, p. 1147–1150, doi:10.1016/0016-7037(86)90396-0.

Sahy, D., Condon, D.J., Hilgen, F.J., and Kuiper, K.F., 2017, Reducing Disparity in Radio-Isotopic and Astrochronology-Based Time Scales of the Late Eocene and Oligocene: Paleoceanography, v. 32, p. 1018–1035.

Schmitz, M.D., and Schoene, B., 2007, Derivation of isotope ratios, errors, and error correlations for U-Pb geochronology using 205Pb-235U-(233U)-spiked isotope dilution thermal ionization mass spectrometric data: Geochemistry, Geophysics, Geosystems, v. 8, no. 8, p. 1–20, doi:10.1029/2006GC001492.

Sláma, J., Košler, J., Condon, D.J., Crowley, J.L., Gerdes, A., Hanchar, J.M., Horstwood, M.S., Morris, G.A., Nasdala, L., Norberg, N., and Schaltegger, U., 2008, Plešovice zircon - A new natural reference material for U-Pb and Hf isotopic microanalysis: Chemical Geology, v. 249, p. 1–35, doi:10.1016/j.chemgeo.2007.11.005.

Ullah, R., Fengjuin, N., Chengyong, Z., Izhar, S., Safdar, I., Xin, Z., and Ali, A., 2020, Occurrence of a Likely Tuff Bed between the Middle and Upper Siwaliks, Taunsa area,

Dera Ghazi Khan, Eastern Sulaiman Range, Pakistan: International Journal of Economic and Environmental Geology, v. 11, p. 24–34.

Vermeesch, P., 2018, IsoplotR: A free and open toolbox for geochronology: Geoscience Frontiers, v. 9, p. 1479–1493, doi:10.1016/j.gsf.2018.04.001.

Watson, E.B., Wark, D.A., and Thomas, J.B., 2006, Crystallization thermometers for zircon and rutile: Contributions to Mineralogy and Petrology, v. 151, no. 4, p. 413–433, doi:10.1007/s00410-006-0068-5.

Wiedenbeck, M., Allé, P., Corfu, F., Griffin, W.L., Meier, F., Oberli, F., von Quadt, A., Roddick, J.C., and Spiegel, W., 1995, Three natural zircon standards for U-Th-Pb, Lu-Hf, trace element and REE analyses: Geostandards Newsletter, v. 19, p. 1–23.